Colloid & Polymer Science Colloid Polym Sci 272:633–654 (1994)

Original Contributions

Transcrystallinity effects in thin polymer films. Experimental and theoretical approach*)

N. Billon, C. Magnet, J. M. Haudin, and D. Lefebvre[1])

Centre de Mise en Forme des Matériaux, Ecole des Mines de Paris, Sophia-Antipolis, France
[1]) Centre de Recherche des Carrières, Rhône-Poulenc, Saint-Fons, France

Abstract: An experimental and theoretical investigation of the overall crystallization kinetics of thin polymer films containing transcrystalline regions on their surfaces is presented. DSC experiments on polyamide 6-6 show that typical features of crystallization curves can be associated with the occurrence of transcrystallinity. In order to interpret these experimental results, a theoretical model is built within the frame of overall crystallization kinetics theories. It makes it possible to correlate the thickness of transcrystalline zone both to the crystallization temperature, the shape of the peak and the density of nuclei within the polymer. Computer simulation is also used to describe the different steps of structure development within a thin film containing transcrystalline regions.

Key words: Crystallization – overall kinetics – transcrystallinity – polymer – spherulite – DSC – PA 6-6

1. Introduction

Polymer crystallization is a two-step phenomenon: first, nucleation of the crystalline phase and then, growth of the semi-crystalline entities (e.g., the spherulites) originating from the nuclei. It can be described in an overall manner by the transformed volume fraction α, which is the volume fraction of polymer overlapped by the entities. This parameter, which ranges from 0 to 1 at the end of the transformation, must not be confused with the crystalline fraction.

It is generally admitted that homogeneous nucleation rarely occurs in polymers. Unlike the homogeneous one, heterogeneous nucleation requires the presence of a foreign surface. A theoretical approach for this type of nucleation has been developed by Binsbergen [1]. If the foreign body initiating the crystallization is a macroscopic surface, a large number of spherulites appear at the contact between this body and the polymer. Due to their proximity, these spherulites lead to what is usually called "transcrystalline regions", in which crystals grow preferentially normal to the surface [2].

The materials leading to transcrystalline effects on polymers can be metals such as aluminum or copper [3–6], other polymers, for instance, polymer fibers [3, 5–13], carbon or glass fibers [13–17] and so on. Although according to Fitchmun and Newman [2], the morphology of transcrystalline regions can be completely explained in terms of geometrical effects resulting from the proximity of heterogeneous nuclei, the effects of a crack on a glass slide [4] or of mechanical stresses [17–20] have been reported. Polymers in which transcrystallinity has been observed are also numerous: polyethylene, polypropylene, polyamides, polyether-ether-ketone, polyphenylene sulphide, polyethylene oxide, etc.

*) Dedicated to Prof. H. Janeschitz-Kriegl, Linz University, on the occasion of his 70th birthday

As a consequence, a huge number of couples polymer-surface has been investigated in the literature and it is difficult to give an exhaustive list.

Transcrystallinity can exist during processing (contact with tools), on reinforcing materials, such as fibers, and on nodules in polymer blends and then, modify the final properties of the product. Most of the recent studies are concerned with composite materials and an open question is: does transcrystallinity improve the mechanical properties, or not? Transcrystallinity can also appear during laboratory characterization (contact with devices, glass slides, DSC pans, etc.) and then disturb measurements.

From a fundamental point of view, an important problem is to explain the nucleating ability of such numerous surfaces. This point is still the object of controversy (see, for instance, [21]). In spite of its evident scientific and technological interest, this is not the purpose of the present paper, which is concerned only with the influence of transcrystallinity on crystallization kinetics.

From an experimental point of view, overall crystallization kinetics are usually determined by differential scanning calorimetry (DSC). In this technique, the polymer is contained in metallic pans, commonly aluminum pans. The nucleating ability of aluminum, or more likely of alumina (Al_2O_3), has already been demonstrated for various polymers [3, 5]. Such an effect has been encountered in DSC analysis of high density polyethylene [8] and polypropylene [22]. For our part, it has been encountered for high density polyethylene, polyamides 6 and 6-6, polybutene-1 (see, for instance, [23]). Therefore DSC appears as a very convenient way to characterize the modifications of the experimental crystallization kinetics induced by transcrystallization. This technique will be applied here to polyamide 6-6 (PA 6-6), which is known to promote important transcrystallinity [23–25].

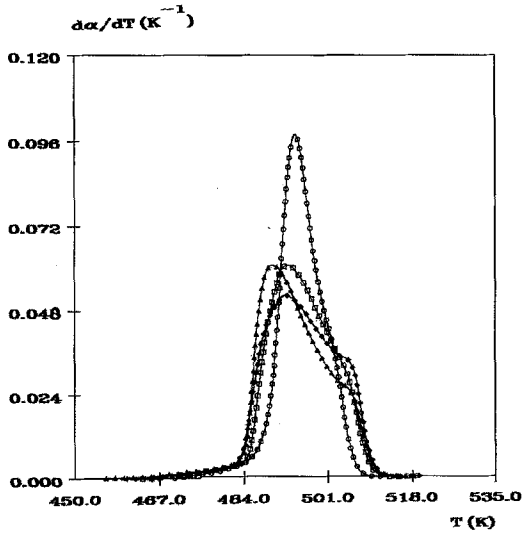

Fig. 1. PA 6-6 DSC crystallization traces for four different specimens cooled from 568 K at the same cooling rate (20 K/min); α is the transformed volume fraction (α = partial area/total area)

In order to explain the experimental DSC results, a theoretical model for the description of overall crystallization kinetics in presence of transcrystallinity will be developed. Computer simulation will also be extensively used.

2. Experimental

2.1. Experimental procedure

The experiments were conducted with a polyamide 6-6 grade supplied by Rhône-Poulenc and usually used in melt spinning: $\overline{M_w} = 19\,800$, $\overline{M_n} = 9000$. The pellets were dried for 16 h at 110 °C, before being melted at 290 °C between two glass slides on a hot-stage Mettler FP 800 and then crystallized in air. Disk-shaped specimens (diameter 6 mm) were cut from these films of calibrated thickness and introduced into aluminum DSC pans.

The DSC samples were heated at 10 K/min in a Perkin Elmer DSC-2 to reach 295 °C, where they were held for 7 min. Then, crystallization experiments were performed under constant cooling rates ranging from 0.3125 to 20 K/min.

Microtomed cross-sections were cut from these samples and observed by transmission optical microscopy between crossed polarizers, using a Reichert Zetopan-Pol microscope.

2.2. Results

DSC traces recorded during cooling at a constant rate give access to $d\alpha/dT$ as a function of temperature T. Figure 1 shows the curves obtained for four different 600-μm-thick specimens

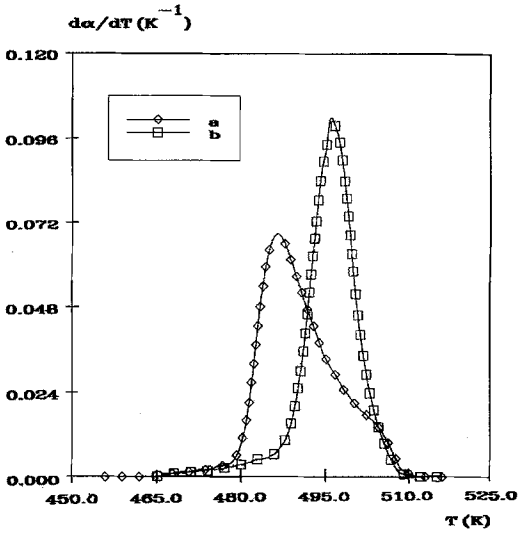

Fig. 2. PA 6-6 DSC crystallization traces for two specimens cooled from 568 K at 20 K/min

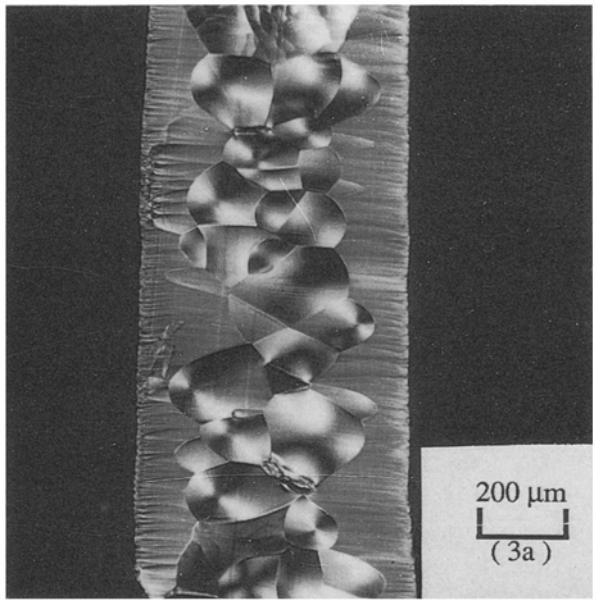

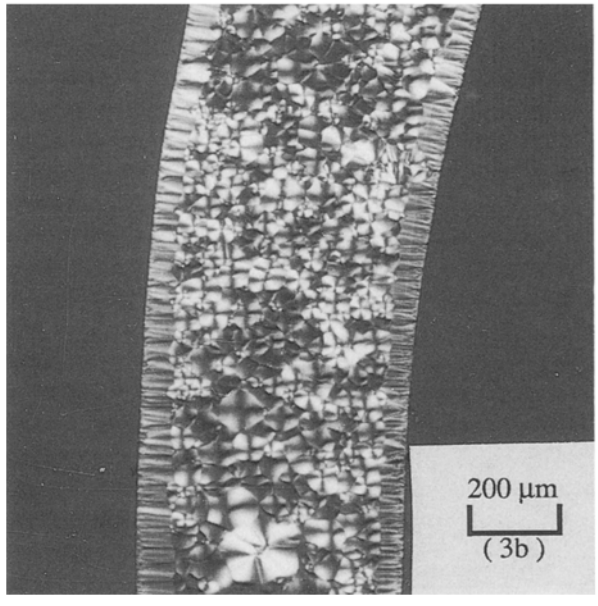

Fig. 3. Microtomed cross-sections of the DSC specimens, whose crystallization traces are displayed in Fig. 2. Figure (3a) corresponds to thermogram (2a) and Fig. (3b) to thermogram (2b)

cooled from 568 K (295 °C) at 20 K/min. The shape of the curves varies significantly from one specimen to another: three curves exhibit a more or less pronounced shoulder, whereas the fourth one shows only a single crystallization peak. All the samples were prepared rigorously using the same procedure presented in Section 2.1. In order to understand the origin of this complex shoulder shape, the morphologies of two specimens crystallized at 20 K/min (using the same procedure) were compared and related to the shape of the thermograms (Figs. 2 and 3). The thermogram (2a) with a shoulder corresponds to a morphology consisting of an important transcrystalline region and coarse spherulites at the specimen core (Fig. 3a). Conversely, the thermogram (2b), which exhibits only a single peak, is associated with a thin transcrystalline region, and a large number of small spherulites at core (Fig. 3b).

Then, a series of 300-μm-thick films was crystallized in the DSC at constant cooling rates ranging from 0.3125 to 20 K/min. The crystallization thermograms exhibit a complex shoulder shape which varies as a function of the cooling rate (Fig. 4): at 20 K/min a small shoulder is observed in the region of high temperatures. As the cooling rate decreases, this initial shoulder seems to become more and more important, and at very low cooling rate, it seems to be the only observable peak. For this series of experiments, transcrystalline regions are present in the specimens, whatever the cooling rate (Fig. 5).

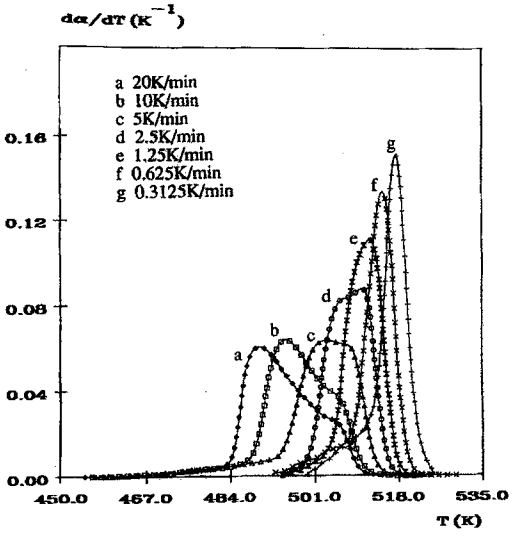

Fig. 4. PA 6-6 DSC crystallization traces recorded during cooling from 568 K at various constant cooling rates

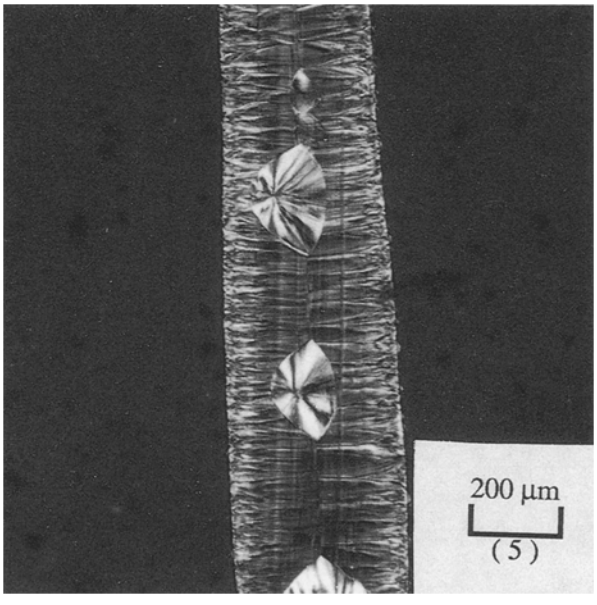

Fig. 5. Morphologies observed in the thickness of the DSC sample corresponding to trace (4d) in Fig. 4 (crystallization at 2.5 K/min)

Finally, Figs. 6 and 7 compare experiments carried out with 600-μm-thick films at two different cooling rates: 10 and 20 K/min. At 10 K/min, the transcrystalline region is larger, the spherulites at the specimen core are coarser, and a small shoulder is observed on the DSC trace.

2.3. Discussion

For the above experimental results, it clearly appears that there is a correlation between the shape of the DSC crystallization curve and the morphology observed at the end of the anisothermal crystallization: a complex shoulder shape can be correlated with a thick transcrystalline region, whereas a single crystallization peak corresponds to a thin one. Furthermore, in the case of a thick transcrystalline region (Figs. 3a and 7b) coarse spherulites are observed inside the films, and on the contrary, numerous small spherulites coexist with a thin transcrystalline zone (Figs. 3b and 7a). This could reflect the competition between surface and volume nucleation.

The shape of the thermogram varies significantly with the cooling rate, but it would be imprudent, at this stage, to draw more precise conclusions about the relationship between cooling rate and extent of transcrystallinity, since for the same cooling rate, different shapes of the thermograms (Figs. 1 and 2) and different morphologies can be obtained (Fig. 3). The reason of this latter fact remains presently unknown and is beyond the scope of this paper.

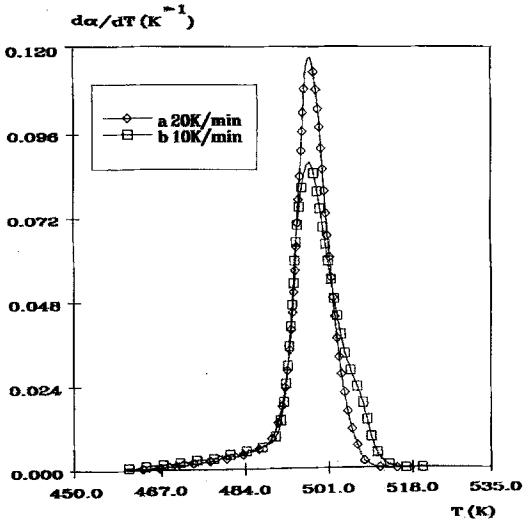

Fig. 6. PA 6-6 DSC crystallization traces for two different cooling rates

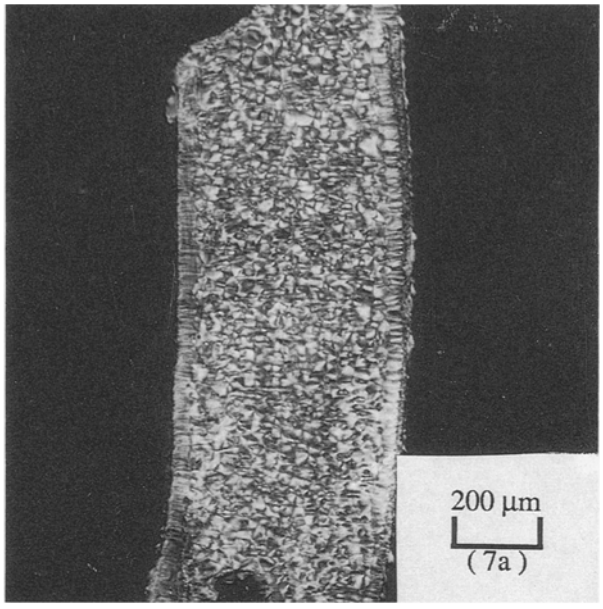

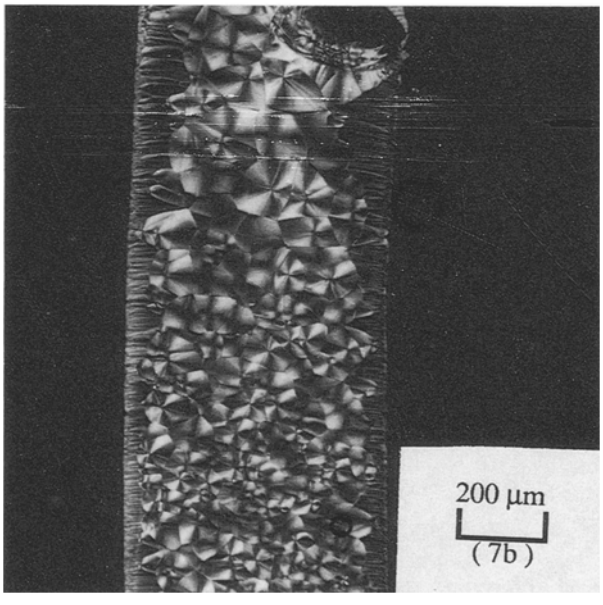

Fig. 7. Crystalline morphologies of the specimens analyzed in Fig. 6. Fig. (7a) corresponds to thermogram (6a) (crystallization at 20 K/min). Fig. (7b) corresponds to thermogram (6b) (crystallization at 10 K/min)

In order to fully understand the shape of the DSC curves and the final morphology, it should be necessary to follow the structure development during the DSC experiment, which is unfortunately impossible. Therefore, this complex problem of structure development was approached in two different ways:

- the use of a theoretical model for overall crystallization kinetics in presence of transcrystallinity. The model will be presented in the following section.
- the use of computer simulation.

3. Theoretical model for overall crystallization kinetics in presence of transcrystallinity

3.1. General outlines of the theory

Our theoretical approach is based on an extension of Evans' theory [26], which has already been published elsewhere [27–30]. In the case where there is only one type of nuclei, the nucleation is described by two parameters: N_0, the initial number of potential nuclei per unit volume, which is defined locally as a function of the spherical coordinates ρ, θ, ϕ, and q, their activation frequency, which depends only on temperature. As soon as it is activated, a potential nucleus becomes a semi-crystalline spherical entity (spherulite), which grows at the radial growth rate G, until it impinges on another entity; G is assumed to depend only on the temperature, which is classical for polymer spherulite.

Furthermore, if temperature is locally uniform, i.e., uniform at the scale of crystallization phenomena, any problem of non-isothermal crystallization can in principle be treated. Nevertheless, an additional assumption will be used here: the isokinetic assumption, in which G/q is assumed to be constant. It is not strictly necessary for the calculations but very useful for their development. Moreover, it is not senseless from a physical point of view since the growth rate of crystalline ribbons is generally assumed to be controlled by secondary nucleation processes [31].

Evans' theory gives the general expression of the average volume fraction of solid entities:

$$\alpha(t) = 1 - \exp[-E(t)] , \qquad (1)$$

where $E(t)$ is the total number of entities which may have passed over a given point in the medium at time t, if these entities are assumed to nucleate and grow independently of each other. Obviously, Eq. (1) takes into account the fact that is is not the case in an actual crystallization: spherulites

cannot overlap one another. Within the frame of the above assumptions $E(t)$ can be written as [27–30]:

$$E(t) = \left[\frac{G}{q}\right]^3 \int_0^{\eta_t} \int_{\theta=0}^{\pi} \int_{\phi=0}^{2\pi} N_0(\rho(\eta_t, \eta_\tau), \theta, \phi) \times [1 - \exp(-\eta_\tau)] \times [\eta_t - \eta_\tau]^2 \sin\theta \, d\phi \, d\theta \, d\eta_\tau \,, \quad (2)$$

where:

$$\eta_t = \int_0^t q(u) \, du \quad (3)$$

and

$$\rho(\eta_t, \eta_\tau) = \frac{G[\eta_t - \eta_\tau]}{q}. \quad (4)$$

When the polymer contains different types of nuclei, which give rise to the same kind of entities growing at the same rate, these different "families" of nuclei can be characterized by their initial densities, $N_{01}, N_{02}, \ldots, N_{0n}$ and their activation frequencies, $q_1, q_2, \ldots, q_n$. Each of them can be considered separately and has a contribution $E^1, E^2, \ldots, E^n$, which can be calculated by means of Eq. (2). The total mathematical expectancy E is given by:

$$E = \sum_{j=1}^{n} E^j \quad (5)$$

3.2. Physical bases of the transcrystallinity model

According to experimental observations [2, 3, 5, 7, 12, 14], transcrystalline regions can be described by the same mechanisms as in the bulk, i.e., by the appearance and the growth of semicrystalline entities. Their number reaches a limit before the end of the transformation and, in some cases, their activation has been modeled using heterogeneous nucleation theory [3, 5, 12]. Therefore, transcrystallinity can be seen as the existence of a large number of additional nuclei on the polymer surface, which could be taken into account in the same way as the volume nuclei, within the framework of classical theories [26, 32–38]. Nevertheless, a major difference is that their distribution is not homogeneous within the volume.

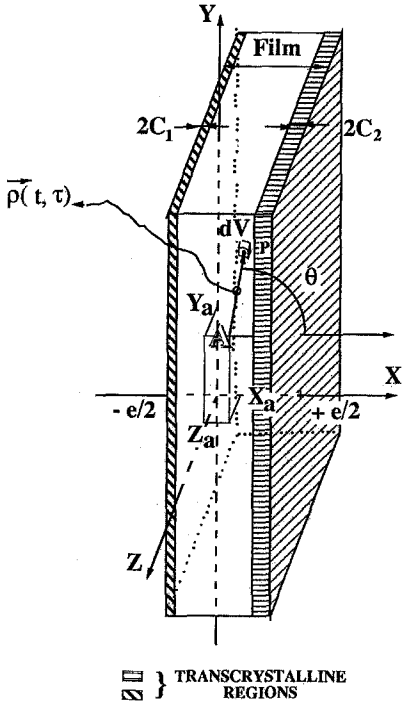

Fig. 8. Representation of the thin film and of its transcrystalline regions

In addition, it must be noticed that the existence of surface nucleation is closely related to the crystallization in a "limited volume", which has been the subject of a number of papers [27–29, 39–41]: the smaller the volume the bigger the influence of surface nucleation. So, these two phenomena (volume limitation and surface nucleation) must be simultaneously taken into account to calculate the evolution of the transformed volume fraction.

As a consequence, a model of the transcrystallization must consider the existence of two kinds of nuclei, which may be non-randomly distributed in a limited volume. This is possible with the extension of Evans' theory we have presented above (see Section 3.1.). This application of the general model will be developed in the following section.

3.3. Modeling of transcrystalline effects

3.3.1. Description: Consider a film of polymer whose thickness is e and a co-ordinate system whose center is the center of the film (Fig. 8).

Assume that both the length and the width of the film are infinite. In presence of transcrystallinity on the surfaces of the film, the nuclei can be organized in two families:

- first, the "volume nuclei" which belong to the polymer and which, in this paper, are assumed to be randomly distributed with the initial density N_0 and the activation frequency q.
- second, the "surface nuclei" which induce the transcrystallinity and which are additional nuclei only distributed close to the surfaces.

Let us assume that the "surface nuclei" are in fact randomly distributed in two very thin regions (Fig. 8), whose thicknesses are $2C_1$ and $2C_2$, respectively, and which are located close to the surfaces of the film. Let N_{0S1} and N_{0S2} be the initial numbers of additional potential nuclei per unit volume in these regions and q_{S1} and q_{S2} their respective activation frequencies.

These three kinds of nuclei give rise to the same type of entities growing at the same rate and then induce the crystallization. The former leads to an E^v contribution to E and the two latter to an E_1^S and an E_2^S contribution. Then,

$$E = E^v + E_1^S + E_2^S \,. \tag{6}$$

The volume contribution E^v is calculated by means of equations established in a previous model [27–29] and presented in Fig. 9. At any time, E^v can be expressed locally at any point of the sample.

3.3.2. *Transcrystallinity contributions to E*:

3.3.2.1 Basic assumptions. If the nuclei are initially distributed at random in the transcrystalline regions, the initial density of "surface potential nuclei" in the whole space is given by (Fig. 10):

$$\begin{cases} N_{0S2}(X) = N_{0S2} & \forall X \in \left[\dfrac{e}{2} - 2C_2, \dfrac{e}{2}\right] \\ N_{0S2}(X) = 0 & \forall X < \dfrac{e}{2} - 2C_2, \text{ or } X \geq \dfrac{e}{2} \\ N_{0S1}(X) = N_{0S1} & \forall X \in \left[-\dfrac{e}{2}, -\dfrac{e}{2} + 2C_1\right] \\ N_{0S1}(X) = 0 & \forall X > -\dfrac{e}{2} + 2C_1 \text{ or} \\ & X \leq -\dfrac{e}{2} \end{cases} \tag{7}$$

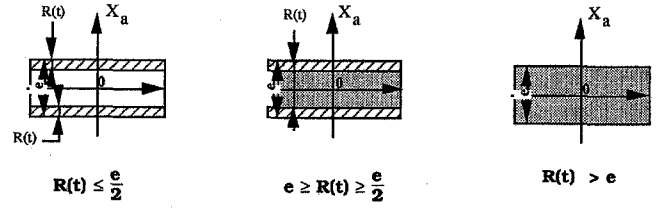

$$E^v(X_a, t) = 8\pi \left[\frac{G}{q}\right]^3 N_0 \, f(\eta_t)$$

$$E^v(X_a, t) = 8\pi \left[\frac{G}{q}\right]^3 N_0 \left[f(\eta_t) + \left(\frac{\gamma}{4} - \frac{1}{2}\right) f(\eta_{Xa}) - \frac{\gamma}{24}\eta_{Xa}^3\right]$$

$$E^v(X_a, t) = 8\pi \left[\frac{G}{q}\right]^3 N_0 \left[f(\eta_t) + \left(\frac{\gamma}{4} - \frac{1}{2}\right) f(\eta_{Xa}) - \frac{\gamma}{24}\eta_{Xa}^3 + \left(\frac{\gamma'}{4} - \frac{1}{2}\right) f(\eta'_{Xa}) - \frac{\gamma'}{24}\eta'^3_{Xa}\right]$$

$$\begin{cases} \gamma = \eta_t - \eta_{Xa} = \dfrac{q}{G}\left(\dfrac{e}{2} - |X_a|\right) \\ \gamma' = \eta_t - \eta'_{Xa} = \dfrac{q}{G}\left(\dfrac{e}{2} + |X_a|\right) \\ f(\eta_t) = \exp(-\eta_t) - 1 + \eta_t - \dfrac{\eta_t^2}{2} + \dfrac{\eta_t^3}{6} \end{cases}$$

Fig. 9. Different values of $E^v(X_a, t)$ according to a previous model [27–29]. $R(t) = \int_0^t G(u)\, du$

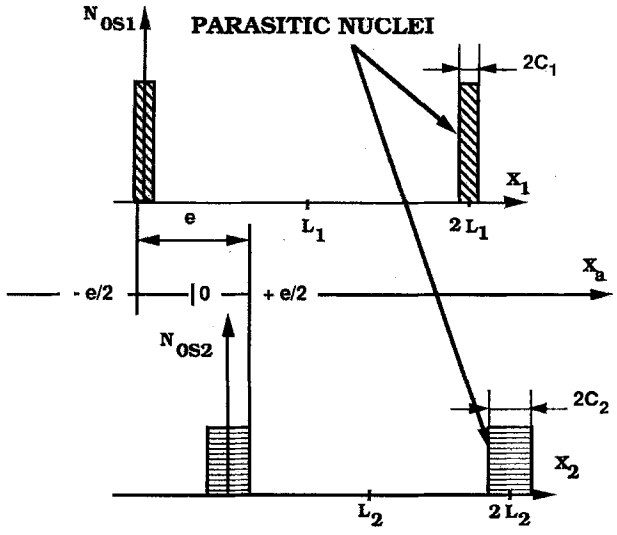

Fig. 10. Representation of the initial distribution of the nuclei which induce transcrystallinity

For the calculations of the mathematical expectancies, E_1^S and E_2^S, relative to each of the transcrystalline regions, such distributions (N_{0Sp} (p equal to 1 or 2)) have been modeled by Fourier series (Fig. 10):

$$N_{0Sp}(X_p) = N_{0Sp}\left(\frac{C_p}{L_p} + \frac{2}{\pi}\sum_{n=1}^{\infty}\frac{1}{n}\sin\left[\frac{n\pi C_p}{L_p}\right] \times \cos\left[\frac{n\pi}{L_p}X_p\right]\right). \quad (8)$$

3.3.2.2 Results. Some details of the calculations are presented in Appendix 1 and the complete results can be found in Reference [29]. Actual transcrystallinity is assumed to be modeled when C_1 and C_2 tend to 0. Our model enables us to consider cases where the transcrystallinity is identical (symmetrical transcrystallinity) on both sides of the film, or not (non-symmetrical transcrystallinity). For simplicity, only the case of symmetrical transcrystallinity will be treated here, since it seems more appropriate in view of our experimental results. The corresponding values of $E^S = E_1^S + E_2^S$ are given in Table 1.

3.4. Model for DSC analysis

Our model enables us to calculate the transformed volume fraction at any point of a thin film:

$$\alpha(X_a, t) = 1 - \exp(-E^v(X_a, t) - E^S(X_a, t)) \quad (9)$$

As DSC samples are thin disks of 300 or 600 μm thickness and 6 mm diameter, it can be assumed that our model is a good approximation for them.

Nevertheless, during experiments $\alpha(X_a, t)$ cannot be determined as a function of X_a. In fact, DSC experiments lead to the mean transformation kinetics which is given by:

$$\left\langle\frac{\partial\alpha(t)}{\partial t}\right\rangle = \frac{2}{e}\int_0^{e/2}\frac{\partial\alpha(X_a, t)}{\partial t}\,dX_a \quad (10)$$

and after integration:

$$\langle\alpha(t)\rangle = \frac{2}{e}\int_0^{e/2}\alpha(X_a, t)\,dX_a\,. \quad (11)$$

These average evolutions are calculated numerically.

Table 1. General expressions of $E^S = E_1^S + E_2^S$ in the case of an actual, symmetrical, surface nucleation

$$\left\{\begin{array}{ll} {}^{S}\gamma_1 = \frac{q_s}{G}\left(\frac{e}{2} - |X_a|\right) & {}^{S}\gamma_2 = \frac{q_s}{G}\left(\frac{e}{2} + |X_a|\right) \\ {}^{S}\eta_{Xa} = \eta_t - {}^{S}\gamma_1 & {}^{S}\eta'_{Xa} = \eta_t - {}^{S}\gamma_2 \end{array}\right\}$$

$$\eta_t = \int_0^t q_s(u)\,du$$

$R(t) \le \frac{e}{2}$	$\lvert X_a\rvert < \left(\frac{e}{2} - R(t)\right)$	$E^S = 0$
	$\lvert X_a\rvert \ge \left(\frac{e}{2} - R(t)\right)$	$E^S = 2\pi\left[\frac{G}{q_S}\right]^2 N_S\left[\left({}^{S}\gamma_1 - 1\right)g\left({}^{S}\eta_{Xa}\right) + \frac{1}{2}{}^{S}\gamma_1\left({}^{S}\eta_{Xa}\right)^2\right]$
$R(t) > \frac{e}{2}$	$\lvert X_a\rvert < \left(R(t) - \frac{e}{2}\right)$	$E^S = 2\pi\left[\frac{G}{q_S}\right]^2 N_S\left[\left({}^{S}\gamma_1 - 1\right)g\left({}^{S}\eta_{Xa}\right) + \frac{1}{2}{}^{S}\gamma_1\left({}^{S}\eta_{Xa}\right)^2 + \left({}^{S}\gamma_2 - 1\right)g\left({}^{S}\eta'_{Xa}\right) + \frac{1}{2}{}^{S}\gamma_2\left({}^{S}\eta'_{Xa}\right)^2\right]$
	$\lvert X_a\rvert \ge \left(R(t) - \frac{e}{2}\right)$	$E^S = 2\pi\left[\frac{G}{q_S}\right]^2 N_S\left[\left({}^{S}\gamma_1 - 1\right)g\left({}^{S}\eta_{Xa}\right) + \frac{1}{2}{}^{S}\gamma_1\left({}^{S}\eta_{Xa}\right)^2\right]$

$$g(\eta) = \left[-\frac{\eta^2}{2} + \eta - 1 + \exp(-\eta)\right]$$

4. Interpretation of the shape of the DSC peaks

4.1. Preliminary calculations using the theoretical model

Due to the "thickness limitation" effects the transformed volume fraction may decrease when it is calculated closer to the surface of the film. The transcrystalline regions act in the opposite way and more or less balance the lack of transformation near the surfaces (Table 1). The average transformed fraction, $\langle\alpha(t)\rangle$ (Eq. (11)), depends on the characteristics of both the volume and the surface nuclei.

As a consequence, the shapes of the crystallization peaks ($\langle\partial\alpha/\partial t\rangle$) may be disturbed. As an example, fictitious DSC peaks have been calculated using the equations of Fig. 9 and Table 1, for several cooling rates. Our model uses both nucleation and growth data. By means of microscopic observations, it is possible to measure G and its variations versus temperature, T. In the case of the polyamide 6-6 envisaged above, if the temperature, T, is in K and the growth rate, G, in μm/s:

$$G = \exp(11.5 \pm 0.3)\exp\left(\frac{-6270}{8.32(T-303)}\right) \times \exp\left(\frac{-(1.89 \pm 0.08)\,10^5}{T(553-T)}\right). \quad (12)$$

Conversely, nucleation parameters are still difficult to determine, even if some attempts have been made in that sense [42, 46]. As a consequence, we have to use arbitrary values for N_0 and G/q.

Nevertheless, it is possible to find sets of parameters such as curves $\langle\partial\alpha/\partial t\rangle$ (or $\langle\partial\alpha/dT\rangle$) versus t (or T) have abnormal shapes with for instance two maxima (Fig. 11). In such a case, the faster the cooling, the more disturbed the shapes of the peaks. These results can be well correlated to our DSC measurements (Fig. 4). In addition, it must be noticed that some authors reported such observations (abnormal peak shapes) in the past on isothermal [6, 10] or anisothermal [9, 10] crystallizations.

4.2. Detailed analysis of the crystallization sequence

At this stage of the investigation, it can be unambiguously concluded that the shoulder

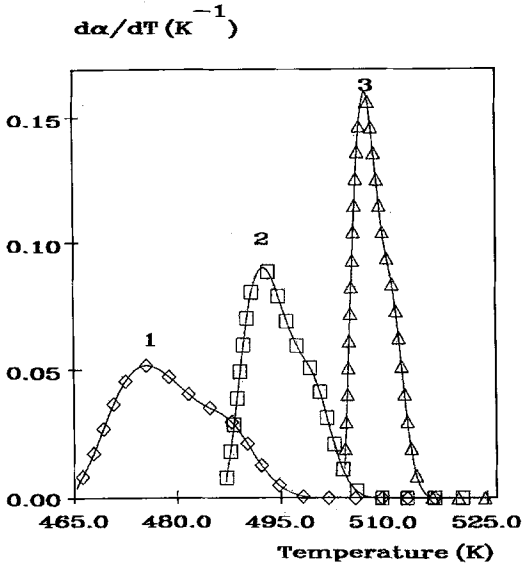

Fig. 11. Plot of $\langle\partial\alpha/\partial T\rangle$ versus temperature T according to our model during anisothermal crystallizations of a 600-μm-thick film. $N_0 = 5\,10^{-5}\ \mu m^{-3}$, $G/q = 1.2\,10^{-5}\ \mu m$, $N_{0S} = 1\ \mu m^{-2}$, $G/q_s = 9.9\,10^{-4}\ \mu m$ and (1) 20 K/min, (2) 5 K/min, (3) 0.3125 K/min

observed on experimental DSC traces must be related to the transcrystalline zone. Therefore, it is interesting to carry out a more detailed analysis in order to identify the respective influences of the surface and volume crystallization on the shape of the DSC curves. This analysis will be based on our theoretical model, but also to a large extent, on computer simulation.

4.2.1. Computer simulation: The computer simulation used in the present paper is an anisothermal extension of a previous isothermal simulation [27, 43]. We consider a parallelepiped in which potential nuclei are randomly distributed, with an initial number per unit volume N_0. These nuclei are activated at random with an average activation frequency q. Both activation time and location of the nuclei are determined using the random number generator of our computer. A potential nucleus which has been overlapped by a previously activated entity cannot be activated. On the contrary, if it is located in a still liquid region, it can be activated and immediately gives rise to a sphere whose growth rate is G. To model transcrystallinity, we introduce additional spherulites, which appear on two parallel surfaces of the

parallelepiped and have different "nucleation characteristics" N_{0S} and q_s.

The program calculates

- the radii of the spherulites,
- their actual shapes, which implies the determination of the boundaries between them,
- and can draw planar sections of the simulated morphologies (in the present case, parallel and perpendicular to the "transcrystalline" surfaces).

4.2.2. Effect of the transcrystalline zones: As the transcrystalline zones are in a general manner visible and continuous (i.e., not interrupted by volume spherulites), it can be inferred that the nuclei from which they originate have a greater activation rate than the volume nuclei. Consequently, at the very first steps of the transformation, the transformed volume consists of distinct semi-spherical spherulites, and if nucleation is assumed to be instantaneous, its expression is, on average:

$$V_t = 2SN_{0S}\frac{2\pi}{3}\left[\int_0^t G(u)\,du\right]^3, \tag{13}$$

where N_{0S} is the density of spherulites existing on the surfaces and S the area of each surface. In consequence, if e is the thickness of the film:

$$\begin{cases} \alpha = \dfrac{4\pi}{3}\dfrac{N_{0S}}{e}\left[\displaystyle\int_0^t G(u)\,du\right]^3 \\ \dfrac{\partial\alpha}{\partial t} = 4\pi\dfrac{N_{0S}}{e}G(t)\left[\displaystyle\int_0^t G(u)\,du\right]^2. \end{cases} \tag{14}$$

Rapidly, as these spherulites grow, they impinge on one another, so that their growth is progressively limited to directions more or less perpendicular to the surfaces. So step by step, the transformed volume becomes "compact". Finally, the transformation results in the growth of two continuous fronts coming from the surfaces. At that moment:

$$\begin{cases} \alpha = \dfrac{2}{e}\left[\displaystyle\int_0^t G(u)\,du\right] \\ \dfrac{\partial\alpha}{\partial t} = \dfrac{2}{e}G(t) \end{cases} \tag{15}$$

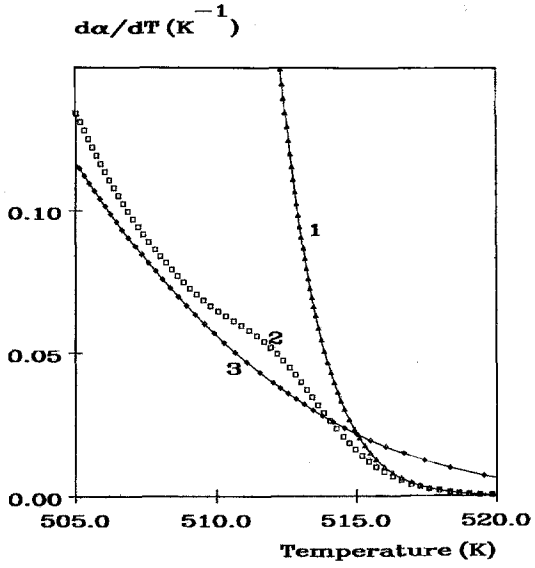

Fig. 12. Comparison between the model (2) in the case where there are no volume spherulites and the growth of distinct half-spheres (1) or continuous crystallizing fronts (3). Thickness 100 μm, cooling rate 10 K/min

Consequently, as surface crystallization proceeds, the transformation rate $\partial\alpha/\partial t$ progressively changes from a form described by Eq. (14) to an expression where it becomes proportional to G (Eq. (15)). This change, which corresponds to a slowing down of the kinetics, is assumed to be responsible for the shoulder observed in the DSC traces (see Section 2).

To demonstrate this fact, our model is compared to the two limiting situations described by Eqs. (14) and (15), in the case of a crystallization at 10 K/min (Fig. 12). For that purpose it is assumed that there are no volume spherulites ($N_0 = 0$) and the growth rate is given by Eq. (12). For convenience, the calculations are performed within the frame of the isokinetic assumption (G/q = constant, see Section 3.1). As the surface entities are supposed to grow at the same rate as the volume ones, this implies that G/q_s is constant. To be close to an instantaneous nucleation considered in Eqs. (14) and (15), values of 10^{-5} μm and 10^{-2} μm^{-2} are chosen for G/q_s and N_{0S}.

Figure 12 shows that at the beginning of the transformation the model is, as expected, close to the case of growing half-spheres (Eq. (14)). Progressively the transformation rate decreases and

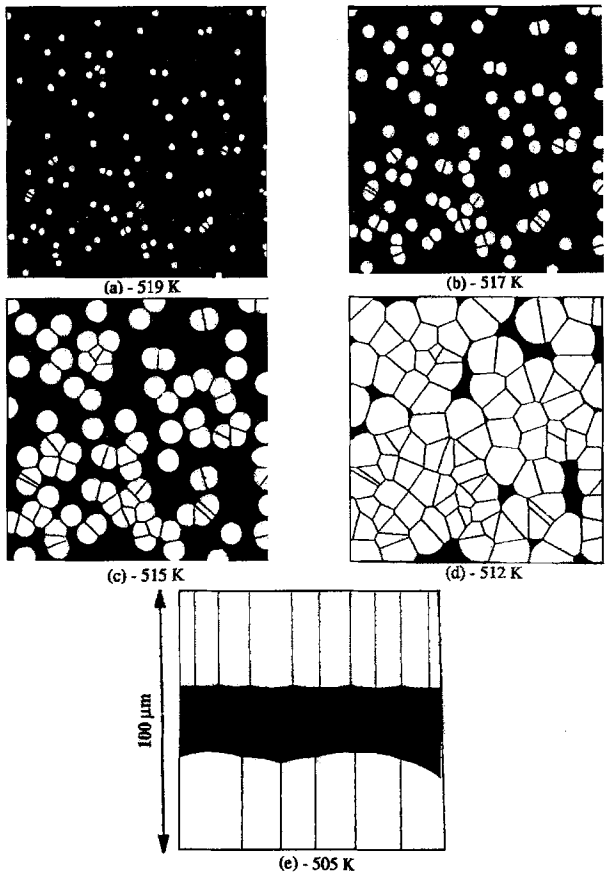

Fig. 13. Computer simulation of the formation of a PA 6-6 transcrystalline zone. Thickness 100 μm, cooling rate 10 K/min. Morphology of a surface before the "shoulder" of the $\partial\alpha/\partial T$ peak (519 K, (a)), at the very beginning of the "shoulder" (517 K, (b)), in the "shoulder" (515 K, (c) and 512 K, (d)), compared to a cross-section after the "shoulder" (505 K, (e))

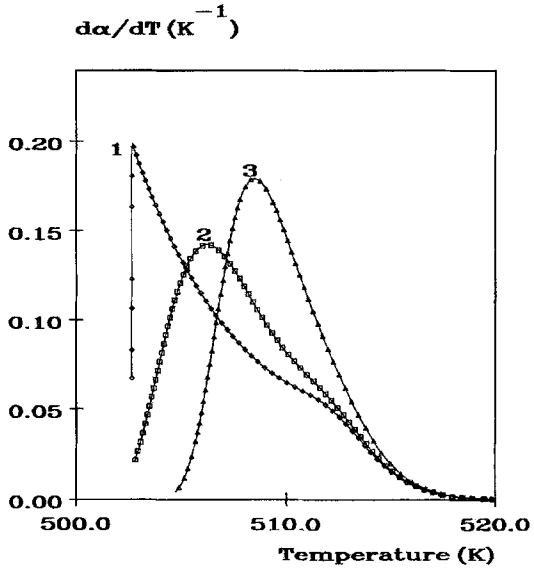

Fig. 14. Model for the crystallization of a 100-μm-thick film without (1) or with volume crystallization ($G/q = 1$ μm, G given by Eq. (12)), $N_{0s} = 10^{-2}$ μm^{-2}, $G/q_s = 10^{-5}$ μm: 2) $N_0 = 5\,10^{-6}$ μm^{-3}; 3) $N_0 = 3\,10^{-5}$ μm^{-3}

then tends to be parallel to the case of a continuous front (Eq. (15)). The shoulder corresponds to the transition zone between these two extreme behaviors. In parallel, a simulation (Fig. 13) clearly demonstrates that before the shoulder the spherulites are essentially distinct half-spheres (Fig. 13(a)). The model gives results different from Eq. (14) in the temperature range where impingements of spherulites begin to occur (Fig. 13(b)). As these impingements are more and more numerous (Figs. 13(c) and (d)) the shoulder is more and more important (curve 2, Fig. 12). Finally, after the shoulder, the transcrystalline regions are continuous (Fig. 13(e)).

This analysis confirms that the shoulder at the beginning of DSC peak can be unambiguously related to the transcrystalline zones. Furthermore, it is due to a change in the transformation kinetics, from half-spheres to continuous fronts.

4.2.3. Effect of bulk nuclei: If volume nuclei are added the shoulder is progressively modified and can even disappear (Fig. 14). Nevertheless, if N_{0s}, q_s, and G are kept constant, the beginning of the peak remains the same.

It must be noticed that the temperature at the maximum of the peak, for its part, depends on N_0 and q. Hence, for the same transcrystallinity parameters, the position of the maximum of the peak is an indication on the volume nucleation.

These effects can be illustrated by additional experiments concerning an injection-molding PA 6-6 grade in which transcrystalline effects are known to be important [44]. When a nucleating agent, promoting volume nucleation, is added to the polymer, the shoulder-shaped peak becomes a single-one, and its maximum is shifted towards higher temperature, as predicted by our model when the number of volume spherulites increases

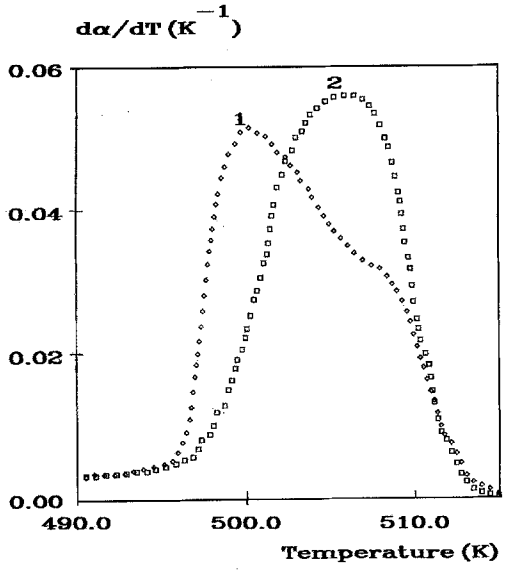

Fig. 15. Experimental DSC peaks at a 10 K/min cooling rate [44]. Comparison between a given polymer (1) and the same polymer with a nucleating agent (2)

(Fig. 15). The same kind of observations can be done on our experiments (See Section 2): The less numerous the volume spherulites the more important the shoulder (Figs. 2, 3, 6, and 7), and the main peak occurs at lower temperature.

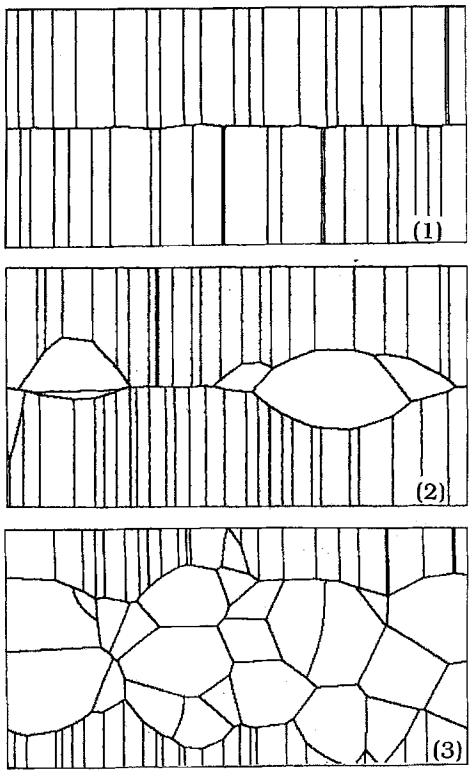

Fig. 16. Simulation of the crystallization of a 100-μm-thick film without (1) or with volume crystallization ($G/q = 1$ μm, G given by Eq. (12)), $N_{0S} = 10^{-2}$ μm^{-2}, $G/q_s = 10^{-5}$ μm: 2) $N_0 = 5\,10^{-6}$ μm^{-3}; 3) $N_0 = 3\,10^{-5}$ μm^{-3}. Visualization of a planar cross-section of the specimen.

5. Thickness of the transcrystalline zones

5.1. Method for the calculation

As it has already been suggested [22], bulk nucleation competes with surface nucleation and the final thickness of the transcrystalline zones is determined by the crystallization rate within the volume, i.e., by the number of volume spherulites since growth rates are identical. This can be experimentally observed (Figs. 3 and 7) or numerically simulated (Fig. 16). The more numerous the bulk nuclei, the thinner the transcrystalline zones. It can also be calculated.

The growth of a transcrystalline zone will be stopped when it impinges on a spherulite which appeared in the volume. As shown before, in the case where the nucleation at the surface is instantaneous, and the number of spherulites is sufficient, the crystallization from the surfaces rapidly behaves as the growth of two continuous fronts. So the bulk crystallization is equivalent to the crystallization of a film whose thickness, e', progressively decreases:

$$e'(t) = e - 2\int_0^t G(u)\,du \tag{16}$$

Locally, along the boundary of the transcrystalline zone, the probability for that zone to be stopped is equal to the probability for the surface of this slice of molten polymer to be transformed. According to our models for crystallization of thin films [27–29, 40, 41] whose major results are recalled in Fig. 9, this probability, which is in fact the transformed volume fraction, is independent of the thickness at the beginning of the transformation and is given by (see Figure 9, for $R(t) \leq e/2$ and $X_a = e/2$):

$$\alpha(t) = 1 - \exp\left(-\frac{E^{\infty}}{2}\right), \tag{17}$$

where E^{∞} is the mathematical expectancy for an infinite volume:

$$\begin{cases} E^{\infty}(t) = 8\pi N_0 \left[\frac{G}{q}\right]^3 \mathbf{f}(\eta_t) \\ \mathbf{f}(\eta_t) = \exp(-\eta_t) - 1 + \eta_t - \frac{\eta_t^2}{2} + \frac{\eta_t^3}{6}. \end{cases} \quad (18)$$

This result is not surprising since, for a point located on the surface at the beginning of the "volume transformation", the film can be regarded as a semi-infinite medium. In such a case, according to the definition of E (Eq. (1)) (number of entities which may reach the considered point), $E = E^{\infty}/2$. Of course, this remains true as long as $R(t)$ is smaller than $e/2$. If the volume crystallization rate is slow enough to ensure that $R(t)$ can be greater than $e/2$, the thickness of the transcrystalline zones, which are assumed to have instantaneous nucleation, is no longer determined by the bulk nucleation but by the thickness of the film itself.

To estimate the average thickness of a transcrystalline zone, $\langle d \rangle$, we have assumed that, at any time t and on an average, the crystallization front grows at a rate G' given by:

$$G'(t) = G(t) \exp\left(-\frac{E^{\infty}}{2}\right). \quad (19)$$

G' is, in fact, G corrected by the probability for the front not to be stopped. As a consequence, the average thickness $\langle d \rangle$ is then given by:

$$\langle d \rangle = \int_0^t G'(u)\, du = \int_0^t G'(u) \exp\left(-\frac{E^{\infty}(u)}{2}\right) du. \quad (20)$$

This estimate is in fact a maximum value since the actual front is not a plane. Nevertheless, results given by Eq. (20) are in very good agreement with the mean values obtained on 100 computer simulation runs (Fig. 17). In such a case the transcrystalline thickness can be defined as the mean value of the surface overlapped by transcrystalline regions divided by the width of the cross-section of the film.

5.2. Temperature at the maximum of the peak and transcrystalline thickness

It has been said that both the position of the maximum of the peak and the thickness of the

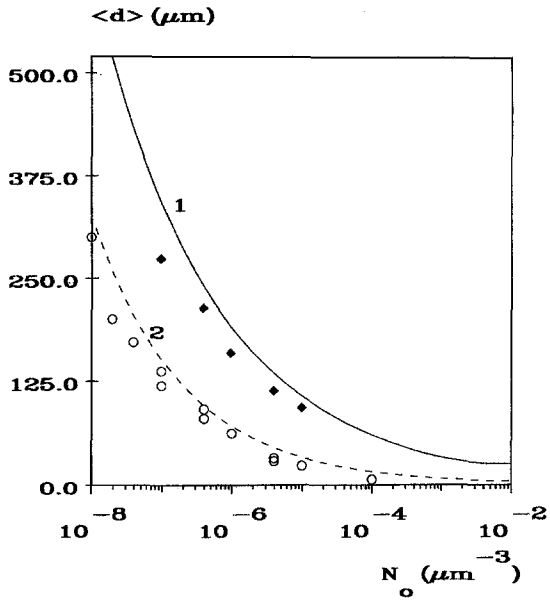

Fig. 17. Thickness of transcrystalline zones. Comparison between our model (Eq. (20)) (solid and dotted lines) and mean values deduced from 100 runs of computer simulation (symbols), as a function of the density of volume nuclei for two activation frequencies: $G/q = 10^3\ \mu m$ ((1) and (◆)) and $G/q = 1\ \mu m$ ((2) and (○)). $N_{0S} = 0.002\ \mu m^{-2}$, $G/q_s = 10^{-5}\ \mu m$

transcrystalline zones depend on N_0 and q, that is, on the nucleation rate. It was then tempting to verify if there is a relationship between this temperature, usually called crystallization temperature T_c, and the thickness $\langle d \rangle$.

Calculations have been performed with values ranging from $10^{-8}\ \mu m^{-3}$ to $10\ \mu m^{-3}$ for N_0 and from $10^{-8}\ \mu m$ to $10^{+8}\ \mu m$ for G/q, for several thicknesses and several cooling rates. It represents about 420 calculations per cooling rate and per thickness. The points representing T_c versus $\langle d \rangle$ are rather well organized in master curves (Fig. 18) depending both on cooling rate and on sample thickness. They are decomposed into two parts:

- a decreasing part where T_c decreases as $\langle d \rangle$ increases,
- a plateau in which T_c does not vary.

This plateau is reached when $\langle d \rangle$ reaches a value close to $e/2$. This means that bulk crystallization is not able to stop transcrystallization which transforms the whole film before any activation within

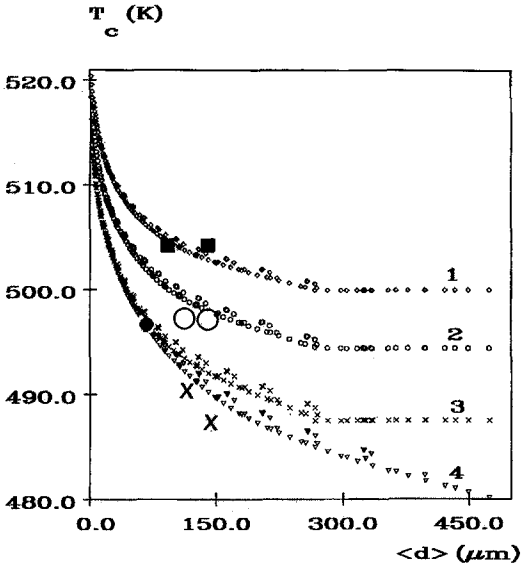

Fig. 18. Evolution of crystallization temperature T_c versus mean transcrystalline thickness $\langle d \rangle$ calculated in four cases (small symbols) and compared to some experimental values (big symbols): 1) and ■, cooling rate 5 K/min, $e = 300$ μm; 2) and ○, cooling rate 10 K/min, $e = 300$ μm; 3) and ●, cooling rate 20 K/min, $e = 300$ μm; 4) and X, cooling rate 20 K/min, $e = 600$ μm

the volume. In such a case T_c is a function of e (transformation stops when $R(t) = e/2$).

If these curves are compared to our experimental results it appears that the agreement is quite good (Fig. 18) if one considers that the calculation gives only a maximum estimate.

6. Estimation of nucleation parameters of a polyamide 6-6

Let us now consider some of our experiments on polyamide 6-6. Assuming that the very beginning of the transformation is due to two instantaneously nucleated transcrystalline zones and using the experimental transformed fraction, α_{exp}, the experimental growth rate (Eq. (12)) and Eq. (14), it is possible to estimate the density of surface nuclei:

$$N_{0S} = \alpha_{exp} \frac{3e}{4\pi} \left[\int_0^t G(u)\, du \right]^{-3} . \qquad (21)$$

Estimates performed on seven cooling rates and for transformed volume fraction smaller than 10% lead to results ranging within a decade: $N_{0S} \in [0.001\ \mu m^{-2}, 0.01\ \mu m^{-2}]$.

Assuming an instantaneous nucleation, our model and experimental values for G and N_{0S} allow to recalculate the beginning of the $d\alpha/dT$ peak, which is mainly due to transcrystallinity. At this stage it must be pointed out that the determination of G and N_{0S} must be as precise as possible, since the calculations are, of course, very sensitive to these parameters. Due to the experimental distribution we have to adjust sets of parameters G and N_{0S} to ensure a good agreement with experiment. Figures 19 and 20 present two of our experimental curves, obtained with different samples whose thicknesses are 300 and 600 μm, respectively. One of the best agreements was found for $N_{0S} = 2\,10^{-3}\ \mu m^{-2}$ and G given by Eq. (12) in the latter case, whereas, in the former, it was found for:

$$\begin{cases} G = 15.37\,10^4 \exp\left(\dfrac{-6270}{8.32(T(K) - 303)}\right) \\ \qquad \times \exp\left(\dfrac{-1.97\,10^5}{T(K)(553 - T(K))}\right) \mu m/s \\ N_{0S} = 1.5\,10^{-3}\ \mu m^{-2} \end{cases} \qquad (22)$$

Despite their difference these values are all in accordance with the experimental distribution for G and N_{0S}.

To recalculate the whole peak, it is also necessary to estimate the volume nucleation parameters, N_0 and q. A first route is to use a trial and error method. Thanks to the T_c versus $\langle d \rangle$ curves (Fig. 18) it is possible to find several sets of parameters N_0 and q giving both the same crystallization temperature and the same transcrystalline thickness (115 μm in the case of Fig. 19). A typical result is shown in Fig. 19. In a general manner, the beginning of the peak, the shoulder, can be well modeled, and the temperature of the maximum of the peak can be reproduced but:

- the solutions are not unique,
- even if the differences observed on the $\partial\alpha/\partial T$ curves (Fig. 19) correspond to differences of less than 20% for α (Fig. 21), the width of the peaks is not satisfactorily predicted.

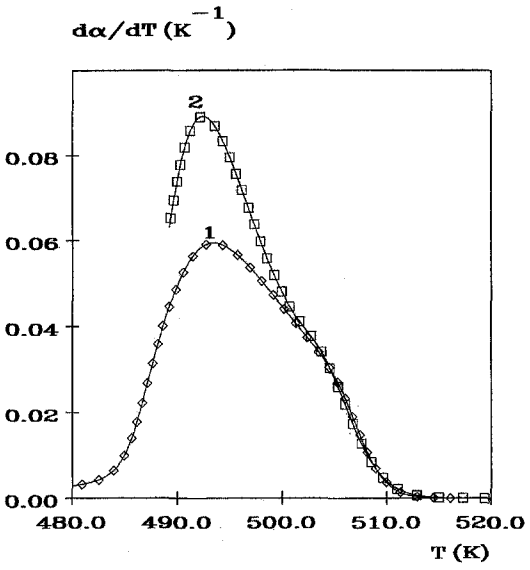

Fig. 19. Comparison between an experimental DSC peak for PA 6-6 (1) and a typical rebuilt peak (2). Cooling rate 20 K/min, G Eq. (22). Thickness 300 μm. $N_{0S} = 1.5\,10^{-3}$ μm^{-2}; $N_0 = 5\,10^{-8}$ μm^{-3}; $G/q_s = 0.1$ μm; $G/q = 1$ μm

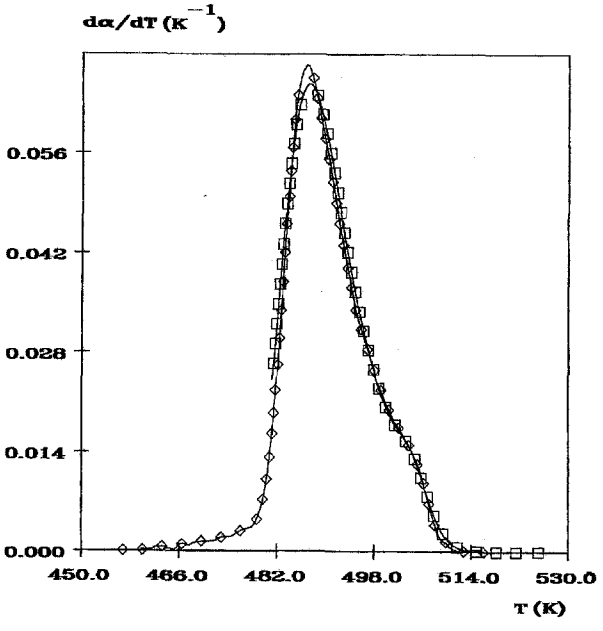

Fig. 20. Comparison between an experimental DSC peak for PA 6-6 (◇) and a recalculated peak (□). Cooling rate 20 K/min, G Eq. (12). Thickness 600 μm. $N_{0S} = 2\,10^{-3}$ μm^{-2}; $N_0 = 2.5\,10^{-8}$ μm^{-3}; $G/q_s = 0.68$ μm; $G/q = 0.6$ μm

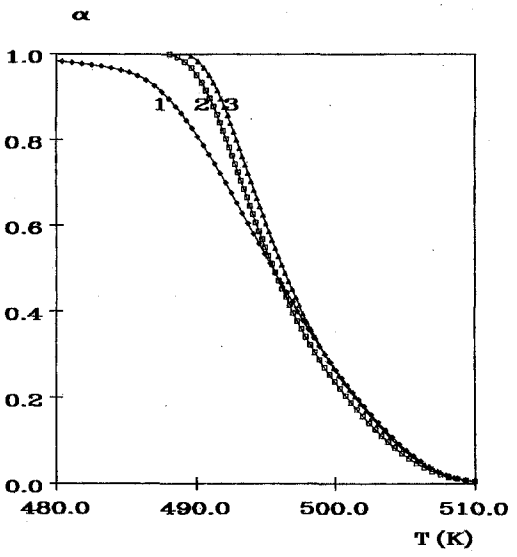

Fig. 21. Comparison between an experimental evolution of α (1) (Fig. 19) for PA 6-6 and typical calculations using G given by Eqs. (12) (2) and (22) (3). Cooling rate 20 K/min

– solutions are very sensitive to the precision on G (Fig. 21).

Another route is to complete purely numerical determinations of N_0 and q by additional data coming from experiments. For instance, it was possible to deduce the value of N_0G/q from the measurement of the activation rate during isothermal experiments [46]. This leads to a set of nucleation parameters, which gives a very good fit of the experimental curve in Fig. 20.

Nevertheless, the parameters determined for Fig. 20 are not able to correctly reproduce the experimental curve of Fig. 19, which corresponds to the same product and the same cooling rate, but to a different experiment. This again raises the problem of the reproducibility of DSC traces for this polymer, which was already mentioned in Section 2 (see, for instance, Fig. 1) and which was beyond the scope of the present paper.

8. Conclusions

Using experimental observations, theoretical approaches and computer simulations, some DSC experiments have been explained. The influence of transcrystallization on measurements, especially

on the shape of the crystallization traces, has been established.

In presence of transcrystallization the crystallization peak can be decomposed into two parts:

- the beginning (shoulder), which is rather representative of transcrystallization,
- the main peak, which is more sensitive to bulk crystallization.

It can be concluded that the shoulder observed in some DSC measurements is directly correlated to transcrystallinity.

Computer simulation makes it possible to visualize the formation of the transcrystalline zones and to show their specific influence on the shape of the crystallization peak. Our model is in very good agreement with simulations. The shoulder, observed on the crystallization trace, can be correlated to a change in transformation kinetics of the transcrystalline zones themselves: the morphology, initially consisting of semi-spherical spherulites, becomes continuous quasi-planar growth fronts. This shoulder will be more or less important depending on the number of surface nuclei, the cooling rate, the thickness of the sample and the volume nucleation. Experiments performed with different cooling rates, on samples of different thicknesses and on nucleated polymers are in excellent agreement with our calculations and simulations.

The maximum of the peak, for its part, is correlated to bulk nucleation even if it is displaced towards higher temperature by transcrystallization. The thickness of the transcrystalline zones is also well correlated to bulk nucleation. As a consequence, it was expected that transcrystalline thickness and crystallization temperature were well correlated together. This was actually proved by computer simulations and experimental observations.

So, our model is in very good agreement from a qualitative point of view with experimental observations. A first attempt for a quantitative interpretation of the data has been proposed.

It is possible to partially fit crystallization peaks according to our model. The shoulder can be correctly rebuilt, the density of surface nuclei can be estimated. The crystallization temperature and the thickness of the transcrystalline zones can be well predicted. Nevertheless, in certain cases, the widths of experimental peaks are greater than those predicted by our model. Experimental dispersion partially explains such a discrepancy, but one must recognize that multiple other reasons for some of our unsatisfactory results can be given.

- The different sets of parameters used in our calculations were generally chosen at random among possible sets. This means that it cannot be ensured that every possible solution has been tested. Nevertheless, even if it is the reason why we did not succeed, it must be noticed that this makes such a method inaccurate. It is impossible to test hundreds of parameters each time a DSC peak is studied. Moreover, the solution in terms of N_0 and q is not unique. It may mean two things:
- either, N_0 and q are not the most convenient parameters to describe the nucleation process, and it would be better to use a combination of them. A solution would be the activation rate (i.e., the number of nuclei activated per unit time). In such a case, the more general formulation of Kolmogoroff [38] should be used instead of Avrami–Evans' theory [26, 32–34], as suggested by some authors [22];
- or, N_0 and q are considered as pertinent parameters, and additional means should be developed to allow their accurate determination. It is encouraging to see that the best fitting of an experimental curve was obtained here from combined numerical and experimental approaches (see Fig. 20). One can also suggest an extension of the method proposed in ref. [42] for 2D-cases. In such a case N_0 and q would be obtained or estimated from optical micrographs of cross-sections of the DSC samples.
- The growth rate, G, is a very important parameter. It is generally measured at high temperatures. Its extrapolation to low temperatures and to the temperature range of DSC crystallization can be erroneous. It is possible to get better results by modifying Eq. (12), especially the term 303 which represents the glass transition temperature minus 30 degrees. This leads to growth rates rather similar at high temperatures, but very different at low temperatures. For the moment, due to a lack of systematic method and theoretical foundation, these modifications must be regarded as mathematical manipulations.

- The physical description of transformation used in overall crystallization kinetics may be insufficient. It should perhaps involve secondary crystallization, or any other phenomenon.
- Thermal gradients within the samples can enlarge crystallization peaks. This is especially true at high cooling rate, but even at 20 K/min perturbations can appear. This can be calculated using anisothermal crystallization models [22, 30, 45], and also by developing models for the DSC calorimeter, including the different thermal resistances [47].

In conclusion, most of the effects of transcrystallinity on DSC measurements have been demonstrated. Some experimental results have been explained and entirely reproduced, but it is not yet possible to easily extract accurate nucleation parameters from experiments when transcrystallization occurs, which is the final aim of such a work. DSC technique should probably be coupled with other determination for nucleation parameters to be more efficient.

In fact it is likely that a good interpretation of DSC measurements needs a complete modeling of the apparatus (thermal gradients, thermal exchange with the furnaces, etc.) as well as a good modeling of the crystallization phenomenon itself. Overall crystallization kinetics theories remain a good way to reach that goal, provided that they are revisited to take into account actual crystallization conditions. We have proposed here ways to take into account both thin samples and transcrystallinity, which have demonstrated their efficiency.

Note added in proof

Overall crystallization theories are statistical approaches. The main difficulty of the calculations is that activations and growths of entities are not independent events, except at the very beginning of the transformation. As a consequence, the exact number of activated entities and their exact shapes are not easily calculated. A rigorous treatment of any crystallization condition should involve elaborate calculations such as those presented here.

Nevertheless, as suggested by one of the referees, there may exist cases where cruder, but simpler, models allow a correct fitting of the experimental curve. For instance, due to the particular location of surface nuclei and to their more efficient nucleation kinetics, it is possible to decompose the transformed volume, V_{tran}, into two volumes:

- V_{sur}, which is overlapped by transcrystalline entities, and
- V_{avr}, which is overlapped by volume entities.

The "transcrystalline volume" can be calculated as the volume overlapped by two continuous planar fronts:

$$V_{sur} = 2\left(\int_0^t G(u)\,du\right)S = 2\,d\,S\,, \tag{N-1}$$

where S is the surface of the film. For its part, V_{avr} can be calculated using the transformed volume fraction, α^∞, given by initial Avrami–Evans' theory:

$$V_{avr} = (e - 2d)\,S\alpha^\infty\,, \tag{N-2}$$

with:

$$\alpha^\infty(t) = 1 - \exp(-E^\infty(t))\,, \tag{N-3}$$

where $E^\infty(t)$ is given by Eq. (18) or by its simplified form:

$$E^\infty(t) = k\eta_t^n \tag{N-4}$$

The total transformed volume, V_{tran}, is the sum of these two contributions: $V_{tran} = V_{sur} + V_{avr}$. Consequently, the transformed volume fraction and its variation are then given by:

$$\begin{cases} \alpha = \dfrac{(V_{sur} + V_{avr})}{eS} = \dfrac{2d}{e} + \alpha^\infty\left(1 - \dfrac{2d}{e}\right) \\ \dfrac{d\alpha}{dt} = \dfrac{2G(t)}{e} - \alpha^\infty\dfrac{2G(t)}{e} + \dfrac{d\alpha^\infty}{dt}\left(1 - \dfrac{2d}{e}\right). \end{cases} \tag{N-5}$$

This remains valid as long as d is lower than $e/2$.

The results given by such a simple model are in a rather good agreement with the complete calculation (Fig. N-1), especially when the main peak is considered. Conversely, the beginning of the peak, particularly the shoulder, disappears in this simplified treatment. The disagreement between the two models is not surprising since the transcrystalline zones are not continuous planar fronts at

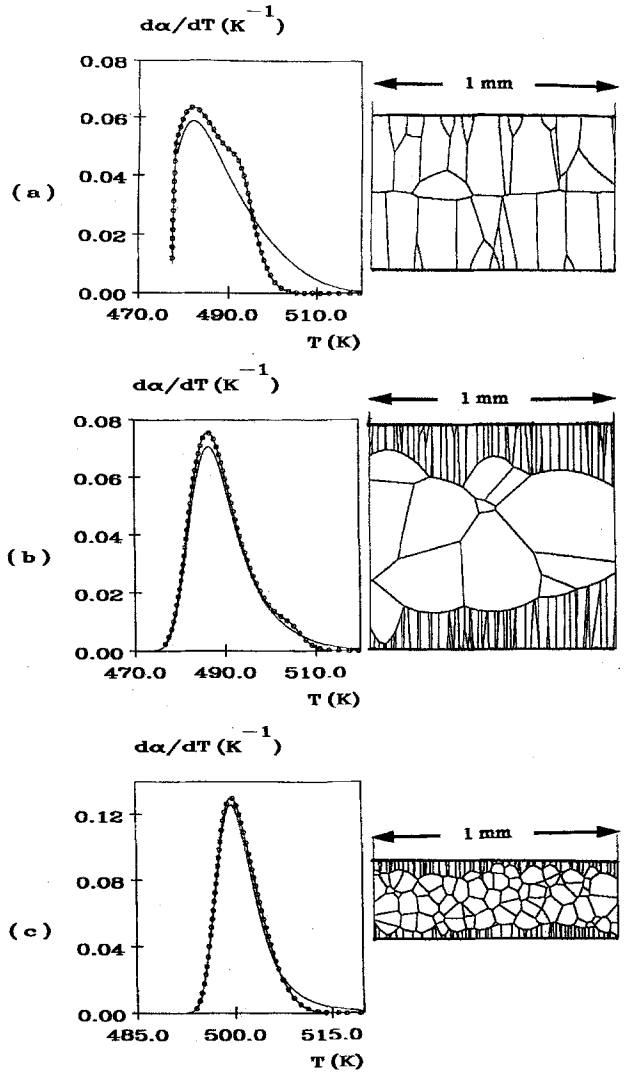

Fig. N-1. Comparison between calculated crystallization peaks obtained with the rigorous model (—○—) and the simple one (Eq. (N-5)) (———), and typical simulated morphologies in different cases (G given by Eq. (12)): a) $N_{0S} = 2\,10^{-3}\ \mu m^{-2}$, $N_0 = 3\,10^{-8}\ \mu m^{-3}$, $G/q_s = 681\ \mu m$, $G/q = 681\ \mu m$, $e = 600\ \mu m$, b) $N_{0S} = 2\,10^{-3}\ \mu m^{-2}$, $N_0 = 3\,10^{-8}\ \mu m^{-3}$, $G/q_s = 0.681\ \mu m$, $G/q = 0.681\ \mu m$, $e = 900\ \mu m$, c) $N_{0S} = 2\,10^{-3}\ \mu m^{-2}$, $N_0 = 3\,10^{-6}\ \mu m^{-3}$, $G/q_s = 0.681\ \mu m$, $G/q = 0.681\ \mu m$, $e = 300\ \mu m$,

the beginning of the transformation. This can be regarded as an additional proof for the above considerations on the relationships between the shoulder shape of the peak and transcrystallinity.

Nevertheless, this simple model may be useful when the relative importance of transcrystallinity is weak, namely, when (Fig. N-1):

- volume and surface nucleations are rather instantaneous;
- the thickness of the sample is sufficient;
- volume nuclei are numerous;
- only the main peak is considered.

Being cautious with the beginning of the peak, we can use Eq. (N-5) to make a first estimate of the volume crystallization kinetics, α^∞, from experimental DSC curves.

Appendix 1

Expression of the E_1^S and E_2^S contributions to E

1. Introduction

Consider a point A having the co-ordinates X_a, Y_a, Z_a and a point P at a distance $\rho(t,\tau)$ from A (Fig. 8). The initial density, $N_{0Sp}(X_a, \rho(t,\tau), \theta)$, of potential nuclei, originating from each surface p ($p = 1$ or 2) and contained in a small volume element dV surrounding P, is given by:

$$N_{0Sp}\left[\frac{C_p}{L_p} + \frac{2}{\pi}\sum_{n=1}^{\infty}\frac{1}{n}\sin\left[\frac{n\pi C_p}{L_p}\right] \times \cos\left[\frac{n\pi}{L_p}\left(X_a - (-1)^p\left(\frac{e}{2} - C_p\right) + \rho(t,\tau)\cos\theta\right)\right]\right]. \quad \text{(A1)}$$

This defines two periodic functions, whose periods are $2L_1$ and $2L_2$, respectively, and which introduce parasitic nuclei in regions centered on points $X_1 = 2L_1$ and $X_2 = 2L_2$ (Fig. 10). These nuclei do not actually exist. Fortunately, they will have no importance for the calculation as long as the fictitious entities they generate do not reach any point, X_a, ranging from $-e/2$ to $+e/2$, that is, as long as

$$R(t) = \int_0^t G(u)\,du < 2L_p - e,\ \forall\, p \in [1,2]\ . \quad \text{(A2)}$$

If L_2 is chosen to ensure that

$$R(t) < 2L_2 - 3e\ , \quad \text{(A3)}$$

$R(t)$ will be smaller than $2L_1 - e$ for any value of L_1, since $L_1 = L_2 - e + C_1 + C_2$. So, the calculation of E^S at any point X_a ranging from $-e/2$ to $+e/2$ will be representative of the film behavior.

2. General E_p^S contribution to E

According to Eq. (2) E_p^S can be written in the general case:

$$E_p^S(X_a, t) = \frac{E_p^{\infty S}}{\beta_p^S} + 8\left[\frac{G}{q_{Sp}}\right]^2 N_{0Sp}\frac{L_p}{\pi}\int_0^{\eta_t^{Sp}} S(p,\zeta) \times\left[1 - \exp\left(\zeta - \eta_t^{Sp}\right)\right]\zeta\, d\zeta\,, \qquad \text{(A4)}$$

with

$$\begin{cases} \eta_t^{Sp} = \int_0^t q_{Sp}(u)\, du \\ S = \sum_{n=1}^{\infty}\frac{1}{n^2}\sin\left[\frac{n\pi C_p}{L_p}\right]\sin\left[\frac{n\pi G}{L_p q_{Sp}}\zeta\right] \\ \quad \times\cos\left[\frac{n\pi}{L_p}\left(X_a - (-1)^p\left(\frac{e}{2} - C_p\right)\right)\right], \end{cases} \qquad \text{(A5)}$$

where $E_p^{\infty S}$ is the value of E_p^S in an infinite volume and $\beta_p^S = L_p/C_p$. Since

$$2\sin\left[\frac{n\pi C_p}{L_p}\right]\sin\left[\frac{n\pi G}{L_p q_{Sp}}\zeta\right] = \cos\left[\frac{n\pi}{L_p}\left(C_p - \zeta\frac{G}{q_{Sp}}\right)\right] - \cos\left[\frac{n\pi}{L_p}\left(C_p + \zeta\frac{G}{q_{Sp}}\right)\right], \qquad \text{(A6)}$$

function S (Eq. (A5)) can be decomposed into two Fourier series:

$$S = \frac{\pi^2(S_1 - S_2)}{4}\,. \qquad \text{(A7)}$$

Functions S_1 and S_2 are periodic functions whose general form is represented in Fig. A-1. They depend on two parameters W_i and A_i

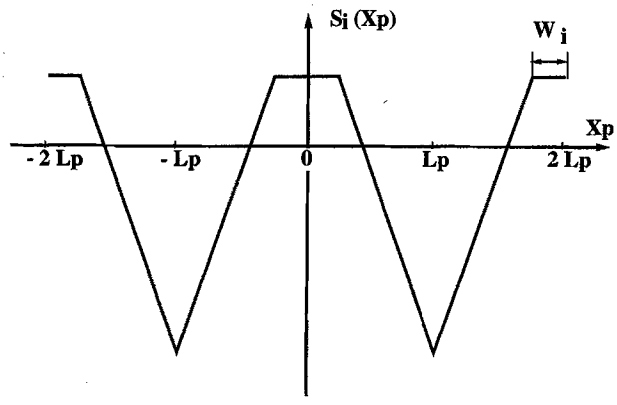

Fig. A-1. General form of the S_i functions

$(i = 1, 2)$:

$$\begin{cases} S_i(X_p) = \frac{2}{\pi^2}\sum_{n=1}^{\infty}\frac{1}{n^2}(\cos[n\pi A_i] - (-1)^n) \times\cos\left[\frac{n\pi}{L_p}X_p\right] \\ X_p = X_a - (-1)^p\left(\frac{e}{2} - C_p\right) \\ A_i = \frac{W_i}{L_p} \\ W_i = C_p + (-1)^i\frac{G}{q_{Sp}}\zeta \\ S_i(0) = \frac{1}{2} - A_i + \frac{A_i^2}{2} \\ S_i(L_p) = -\frac{1}{2} + A_i^2\,. \end{cases} \qquad \text{(A8)}$$

Depending on ζ, parameters W_i and A_i vary. Therefore, as a function of time, S_1 and S_2 have different forms (Fig. A-2). Equation (A4) could then be integrated, but the calculations are long and the results depend on C_1 and C_2 values. For simplicity, we will only consider the case where C_1 and C_2 are very small.

3. Actual surface nucleation

When the transcrystallinity phenomenon is actually a surface effect (C_p close to zero) a density of nuclei per unit surface N_{Sp} can be defined

$$N_{Sp} = 2C_p N_{0Sp} \qquad \text{(A9)}$$

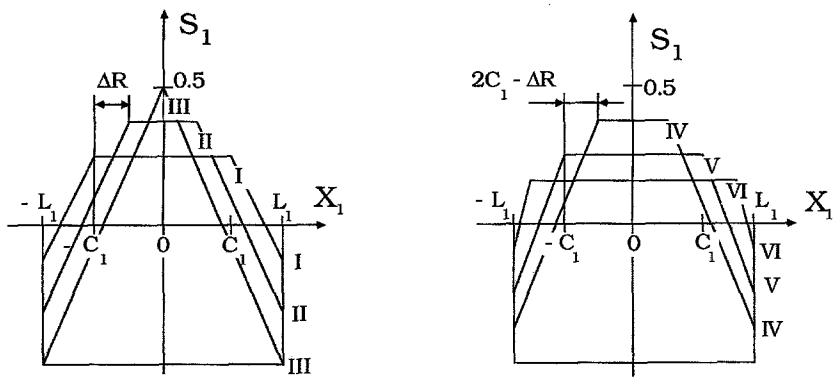

Fig. A-2. Plot of function S_1 for different ζ values. $\Delta R = \frac{G}{q_{s1}}\zeta$. $X_1 = X_a + (\frac{e}{2} - C_1)$. (I) $\Delta R = 0$, (II) $C_1 > \Delta R > 0$, (III) $\Delta R = C_1$, (IV) $2C_1 > \Delta R > C_1$, (V) $\Delta R = 2C_1$, (VI) $\Delta R > 2C_1$

and E_p^S (Eq. (A4)) can be rewritten:

$$E_p^S(X_a, t) = \frac{E_p^{\infty S}}{\beta_p^S} + 4\left[\frac{G}{q_{Sp}}\right]^2 N_{Sp} \int_0^{\eta_t^{Sp}} S'(p, \zeta) \times \left[1 - \exp\left(\zeta - \eta_t^{Sp}\right)\right]\zeta \, d\zeta \quad \text{(A10)}$$

with:

$$\begin{cases} \dfrac{E_p^{\infty S}}{\beta_p^S} = \dfrac{2\pi}{L_p}\left[\dfrac{G}{q_{Sp}}\right]^3 N_{Sp} \times \displaystyle\int_0^{\eta_t^{Sp}} \left[1 - \exp\left(\zeta - \eta_t^{Sp}\right)\right]\zeta^2 \, d\zeta \quad \text{(A11)} \\ S' = \displaystyle\sum_{n=1}^{\infty} \frac{1}{n} \sin\left[\frac{n\pi G}{L_p q_{Sp}}\zeta\right] \cos\left[\frac{n\pi}{L_p} X_p\right]. \end{cases}$$

The half-period L_p has been chosen to ensure that $R(t)$ will always be smaller than $2L_p - e$. Furthermore, as L_p is only a mathematical parameter, it can be chosen greater than e. So, $R(t)$ will always be smaller than L_p, and:

$$\frac{G}{q_{Sp}}\zeta < L_p . \quad \text{(A12)}$$

It follows that S' is a periodic function of X_a whose period is $2L_p$ (Fig. A-3), and such as:

$$\begin{cases} S' = \left(1 - \dfrac{G\zeta}{L_p q_{Sp}}\right)\dfrac{\pi}{2} \\ \forall X_a \in \left[(-1)^p \dfrac{e}{2}, (-1)^p\left(\dfrac{e}{2} - \dfrac{G\zeta}{q_{Sp}} - C_p\right)\right] \quad \text{(A13)} \\ S' = -\dfrac{G\zeta}{L_p q_{Sp}}\dfrac{\pi}{2} \; \forall |X_a| < \left(\dfrac{e}{2} - \dfrac{G\zeta}{q_{Sp}} - C_p\right). \end{cases}$$

The two transcrystalline regions induce crystallizations which disturb the kinetics of the transformation of the film. At any point of the film two times can be defined:

- first, the instant when the crystallization at the point is disturbed by the nearest transcrystalline region;
- second, the instant when at this point the crystallization is disturbed by the furthest region.

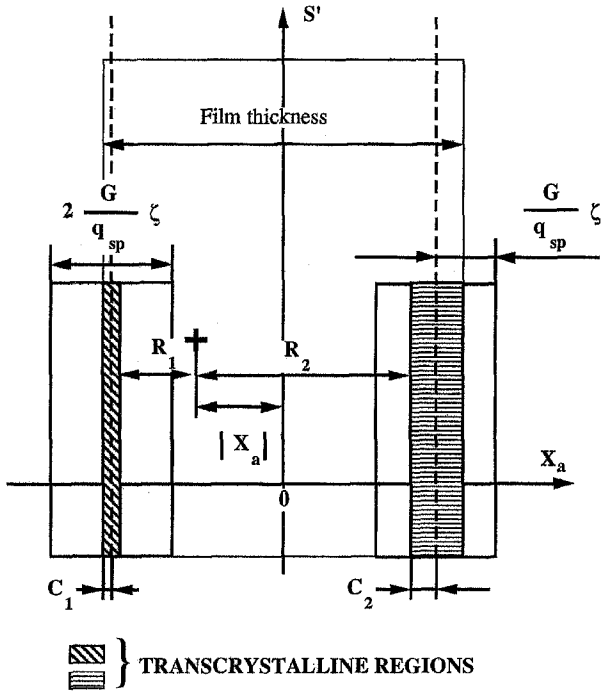

Fig. A-3. Actual surface nucleation. Plot of function S' versus X_a

E_1^S	
$X_a \geq -\frac{e}{2} + R(t) + C_1$	$X_a < -\frac{e}{2} + R(t) + C_1$
0	$\frac{E_1^{\infty S}}{\beta_1^S}$ $-\frac{2\pi}{L_1}\left[\frac{G}{q_{S1}}\right]^3 N_{S1} \int_0^{\gamma_1^{S1}} \left(1 - \exp\left(\zeta - \eta_t^{S1}\right)\right)\zeta^2 d\zeta$ $+ 2\pi\left[\frac{G}{q_{S1}}\right]^2 N_{S1} \int_{\gamma_1^{S1}}^{\eta_t^{S1}} \left(1 - \frac{G\zeta}{q_{S1}L_1}\right)\left(1 - \exp\left(\zeta - \eta_t^{S1}\right)\right)\zeta\, d\zeta$

Table A-1. Expressions of E_1^S before integration as a function of negative X_a

E_2^S	
$R(t) \geq \frac{e}{2} - C_2$	
$X_a < \frac{e}{2} - R(t) - C_2$	$X_a \geq \frac{e}{2} - R(t) - C_2$
0	$\frac{E_2^{\infty S}}{\beta_2^S}$ $-\frac{2\pi}{L_2}\left[\frac{G}{q_{S2}}\right]^3 N_{S2} \int_0^{\gamma_2^{S2}} \left(1 - \exp\left(\zeta - \eta_t^{S2}\right)\right)\zeta^2 d\zeta$ $+ 2\pi\left[\frac{G}{q_{S2}}\right]^2 N_{S2} \int_{\gamma_2^{S2}}^{\eta_t^{S2}} \left(1 - \frac{G\zeta}{q_{S2}L_2}\right)\left(1 - \exp\left(\zeta - \eta_t^{S2}\right)\right)\zeta\, d\zeta$

Table A-2. Expressions of E_2^S before integration as a function of negative X_a.

Let us, for instance, consider a point with an abscissa $X_a \leq 0$ (Fig. A-3). We can define the two characteristic times, $t_1^{S1}(X_a)$ and $t_2^{S2}(X_a)$, so that:

$$\begin{cases} R_1 = R(t_1^{S1}) = \dfrac{e}{2} + X_a - C_1 \\ R_2 = R(t_2^{S2}) = \dfrac{e}{2} - X_a - C_2 \,. \end{cases} \tag{A14}$$

According to these times other parameters, γ_n^{Sp}, can be defined:

$$\gamma_n^{Sp} = \frac{q_{Sp}}{G} R(t_n^{Sp}) \,. \tag{A15}$$

Equation (A4) can then be integrated. When E_1^S is considered, at any time the left half-film ($X_a \leq 0$) is decomposed into two parts (Table A-1):

- the part which is disturbed by transcrystalline region 1 ($E_1^S \neq 0$);
- the undisturbed part ($E_1^S = 0$).

The relative importance of each of them depends on the time t. For its part, E_2^S is equal to 0 in the left half-film as long as:

$$R(t) < \frac{e}{2} - C_2 \,, \tag{A16}$$

that is, at the beginning of the crystallization. When $R(t)$ is greater than $(e/2) - C_2$, the left half-film ($X_a \leq 0$) is disturbed by the second transcrystalline region and can again be decomposed into two parts (Table A-2). The same demonstration can be done for the right half-film ($X_a \geq 0$) and E_S is equal to $E_1^S + E_2^S$. The results are presented in ref. [29].

In the particular case where C_1 and C_2 are both equal to zero and when the transcrystallinity is the same on both sides of the film ($q_{S1} = q_{S2} = q_S$, $N_{S1} = N_{S2} = N_S$, $\gamma_n^{Sp} = \gamma_n^S$) our results (Table 1) can be regarded as an anisothermal generalization of previous models [41].

References

1. Binsbergen FL (1973) J Polym Sci, Polym Phys Ed 11:117
2. Fitchmun DR, Newman S (1970) J Polym Sci A-2 8:1545
3. Chatterjee AM, Price FP (1975) J Polym Sci, Polym Phys Ed 13:2369
4. Shaner JR, Corneliussen RD (1972) J Polym Sci, Polym Phys Ed 10:1611
5. Chatterjee AM, Price FP (1975) J Polym Sci, Polym Phys Ed 13:2391
6. Kantz MR, Corneliussen RD (1973) J Polym Sci, Polym Lett Ed 11:279

7. Gray DG (1974) J Polym Sci, Polym Lett Ed 12:509
8. Kamal MR, Chu E (1983) Polym Eng Sci 23:27
9. Huson MG, Mc Gill WJ (1984) J Polym Sci, Polym Chem Ed 22:3571
10. He T, Porter RS (1988) J Appl Polym Sci 35:1945
11. Yu Z, Ait-Kadi A, Brisson J (1991) Polym Eng Sci 31:1228
12. Campbell D, Qayyum MM (1980) J Polym Sci, Polym Phys Ed 18:83
13. Thomason JL, Van Rooyen AA (1992) J Mater Sci 27:889
14. Lee YC, Porter RS (1986) Polym Eng Sci 26:633
15. Caramaro L, Chabert B, Chauchard J (1991) Polym Eng Sci 31:1279
16. Hsiao BS, Chen EJH (1990) Mat Res Soc Symp Proc: 170
17. Chabert B, Chauchard J (1991) Ann Chim Fr 16:173
18. Thomason JL, Van Rooyen AA (1992) J Mater Sci 27:897
19. Monasse B (1992) J Mater Sci 27:6047
20. Gray DG (1974) J Polym Sci, Polym Lett Ed 12:645
21. Devaux E (1992) Thesis, Université "Claude Bernard" Lyon I
22. Janeschitz-Kriegl H (1992) Progr Colloid Polym Sci 87:117
23. Haudin JM, Billon N, Monasse B (1990) Initiation à la chimie et à la physico-chimie macromoléculaires, Matériaux composites à base de polymères, Groupe Français d'Etudes et d'Applications des Polymères (G F P), Strasbourg, 7:315
24. Billon N, Magnet C, Haudin JM (1992) Eighth Annual Meeting of the Polymer Processing Society, New Delhi
25. Zupko HM (1971) Macromolecules 4:761
26. Evans UR (1945) Trans Faraday Soc 41:365
27. Billon N (1987) Thesis, Ecole Nationale Supérieure des Mines de Paris
28. Billon N, Haudin JM (1989) Colloid Polym Sci 267:1064
29. Billon N, Haudin JM (1990) Ann Chim Fr 15:173
30. Haudin JM, Billon N (1992) Progr Colloid Polym Sci 87:132
31. Mandelkern L (1964) Crystallization of polymers, McGraw Hill, New York
32. Avrami M (1939) J Chem Phys 7:1103
33. Avrami M (1940) J Chem Phys 8:212
34. Avrami M (1941) J Chem Phys 9:177
35. Tobin MC (1974) J Polym Sci, Polym Phys Ed 12:399
36. Tobin MC (1976) J Polym Sci, Polym Phys Ed 14:2253
37. Tobin MC (1977) J Polym Sci, Polym Phys Ed 15:2269
38. Kolmogoroff AN (1937) Izvest Akad Nauk SSR, Ser Math 1:335
39. Stein RS, Powers J (1962) J Polym Sci 56:S9
40. Escleine JM, Monasse B, Wey E, Haudin JM (1984) Colloid Polym Sci 262:306
41. Billon N, Escleine JM, Haudin JM (1989) Colloid Polym Sci 267:668
42. Billon N, Haudin JM (1993) Colloid Polym Sci 271:343
43. Billon N, Haudin JM (1990) Ann Chim Fr 15:1
44. Pretel FD (1991) Internal Report, Mastère MATMEF, Ecole Nationale Supérieure des Mines de Paris
45. Billon N, Barq Ph, Haudin JM (1991) Int Polym Proc 6:348
46. Magnet C (1993) Thesis, Ecole Nationale Supérieure des Mines de Paris
47. Wu CH, Eder G, Janeschitz-Kriegl H (1993) Colloid Polym Sci 271:1116

Received June 28, 1993;
accepted October 5, 1993

Authors' address:

N. Billon
Ecole Nationale Supérieure des Mines de Paris
Centre de Mise en Forme des Matériaux
Unité de Recherche Associée au CNRS N° 1374
BP 207, 06904 Sophia-Antipolis Cedex (France)